

Acknowledgements We thank S. Allan, L. Campbell, L. Chikhi, M. Corballis, N. Gavey, S. Greenhill, J. Hamm, J. Huelsenbeck, G. Nichols, A. Rodrigo, F. Ronquist, M. Sanderson and S. Shennan for useful advice and/or comments on the manuscript.

Competing interests statement The authors declare that they have no competing financial interests.

Correspondence and requests for materials should be addressed to R.G. (rd.gray@auckland.ac.nz).

Contributions of microbial biofilms to ecosystem processes in stream mesocosms

Tom J. Battin¹, Louis A. Kaplan², J. Denis Newbold² & Claude M. E. Hansen³

¹Department of Limnology, IECB, University of Vienna, A-1090 Vienna, Austria

²Stroud Water Research Center, Avondale 19311 Philadelphia, USA

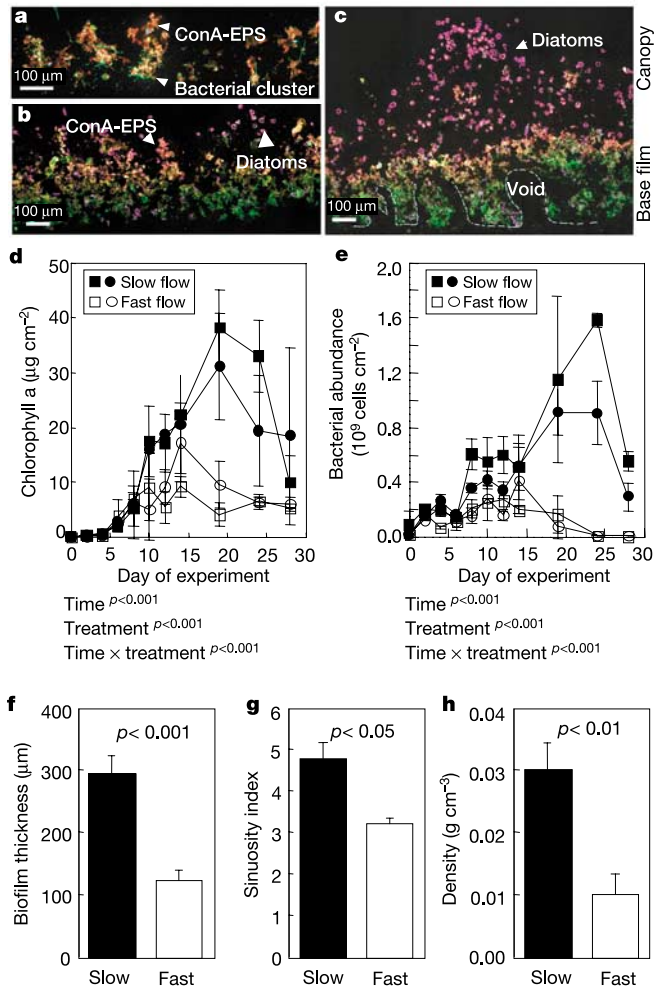
³Institute of Limnology and Zoology, University of Innsbruck, A-6020 Innsbruck, Austria

In many aquatic ecosystems, most microbes live in matrix-enclosed biofilms^{1–3} and contribute substantially to energy flow and nutrient cycling. Little is known, however, about the coupling of structure and dynamics of these biofilms to ecosystem function². Here we show that microbial biofilms changed the physical and chemical microhabitat and contributed to ecosystem processes in 30-m-long stream mesocosms. Biofilm growth increased hydrodynamic transient storage—streamwater detained in quiescent zones, which is a major physical template for ecological processes in streams^{4,5}—by 300% and the retention of suspended particles by 120%. In addition, by enhancing the relative uptake of organic molecules of lower bioavailability, the interplay of biofilm microarchitecture and mass transfer changed their downstream linkage. As living zones of transient storage, biofilms bring hydrodynamic retention and biochemical processing into close spatial proximity and influence biogeochemical processes and patterns in streams. Thus, biofilms are highly efficient and successful ecological communities that may also contribute to the influence that headwater streams have on rivers, estuaries and even oceans^{6,7} through longitudinal linkages of local biogeochemical and hydrodynamic processes.

Although the broad physical factors that influence ecological processes at the streambed interface have been extensively studied^{4,5,8}, the interactions of underlying biological, chemical and physical mechanisms operating at the microscale have not. To investigate whether biofilm growth changes hydrodynamic transient storage and organic matter processing at the streambed/streamwater interface we experimented with natural microbial biofilms in duplicate streamside flumes under two open-channel flow velocities (Methods and Supplementary Information). In both flow treatments, initial biofilms consisted of largely bacterial microcolonies that rapidly coalesced into a basal geometric film surrounding conspicuous voids (Fig. 1). Diatoms became a major component in mature biofilms, and long streamers (filamentous structures) oscillating in the water flow developed in these biofilms. Flow significantly affected biofilm development, yielding higher biomass under slower flows. Biofilm detachment and invertebrate grazing dramatically decreased biomass after day 14 in fast flow and day 25 in slow flow. Confocal microscope analyses of biofilm cryosections (*x-z* plane) revealed that flow also shaped biofilm microarchitecture beyond bulk biomass. Biofilms grown in slow flow developed clearly

visible skins of diatoms, and were thicker with higher surface sinuosity and elevated density than biofilms grown in the fast-flow treatment.

Transient storage has typically been associated with physical structures such as the interstices within streambed sediments or quiescent waters in back eddies, pools and side channels^{4,5}. Although others^{9,10} have indicated the potential for algal-dominated biofilms to influence stream hydrodynamics, we have quantified biofilms as a significant component of the transient storage zone in the stream mesocosms. To do so, we estimated A_s , the cross-sectional area of transient storage (in m^2 , see Methods) and compared it to the cross-sectional areas of the total biofilm, including the biofilm voids. At day 0 (that is, no biofilms) A_s was entirely due to the flume bed, and differences between treatments were attributable to different flow velocities. As microbial growth progressed, transient storage increased 4- and 2.3-fold in the slow- and fast-flow treatments, respectively (Fig. 2). This increase closely followed the temporal pattern of biofilm dynamics, with chlorophyll *a* and organic matter together explaining 76% of the variance in A_s (multiple linear regression, MLR: degrees of freedom,



d.f. = 22, $p < 0.01$). Unlike A_s , the hydraulic exchange velocity—the piston flow into transient storage—was higher in the fast flows. Yet within each treatment, it followed a temporal pattern similar to that of A_s . Cross-sectional areas (m^2) of the total biofilm ($r^2 = 0.81$, d.f. = 10, $p < 0.001$) and of biofilm voids as derived from porosity ($r^2 = 0.89$, d.f. = 10, $p < 0.001$) correlated with the added transient storage zone (m^2) (that is, A_s corrected for the storage zone generated by the flume bed at day 0). Total biofilm and biofilm void cross-sectional areas were respectively, 33% and 16% as large as the added transient storage zone. This indicates that both the internal biofilm channel system (see voids, Fig. 1c) and the highly hydrated³ matrix constitute important transient storage zones—and that the increased transient storage not only contains the growing biofilms, but extends beyond them. The relationship ($r^2 = 0.56$, d.f. = 10, $p < 0.01$) between transient storage and biofilm surface sinuosity suggests how microarchitecture increases transient storage around biofilms. Protuberances at the biofilm surface and streamers could generate vortices that create additional transient storage, which in turn influences the delivery of solutes from the water column to the biofilms. If the oscillation of streamers actually enhances mass transfer within biofilms¹¹, it is likely that oscillating streamers from biofilms covering an entire streambed would collectively increase hydrodynamic exchange at the streambed interface. This underscores the ecological significance of the microbial-altered transient storage.

As biofilm growth altered the hydrodynamic environment in the flumes, it simultaneously increased the deposition velocity of suspended organic particles (Fig. 3a). Particle deposition was predicted best from the hydraulic exchange velocity and accumulation of microbial exopolysaccharides (MLR: $r^2 = 0.78$, d.f. = 16, $p < 0.001$). Hydraulic exchange velocity has been shown to influence inorganic, physicochemical particle deposition in streams⁸, but

our studies found that the hydraulic exchange velocity was five- to eightfold lower than the particle deposition velocity (compare Figs 2b and 3a). This indicates that advective delivery could not have accounted for most of the deposition. Thus, the relationship between microbial growth and deposition provides evidence that biofilm stickiness³ is an important biological influence on particle deposition in streams. This may account for hitherto unexplained variability in measurements of particle deposition^{12,13}. Furthermore, there was a positive relationship ($r^2 = 0.72$, d.f. = 7, $p = 0.01$) between biofilm microarchitecture (as sinuosity) and particle deposition. Our finding that complex surfaces with small streamers or mushroom-shaped features enhance particle retention agrees with the few existing results from laboratory-grown bacterial biofilms¹⁴.

Biofilm theory^{15,16} holds that solute retention, or the uptake of organic substrates as a source of carbon and energy, is diffusion limited. Before assimilation, solutes must pass first from the bulk liquid to the biofilm surface (external mass transfer) and then through the biofilm matrix to the cells (internal mass transfer). Consequently, as biofilms grow, mass transfer may become the primary rate-limiting step because substrate consumption and biofilm structure increase resistance to transport. To determine how biofilm growth influences solute uptake, we measured mass transfer coefficients (V) for the uptake from the water column of glucose and arabinose—two monomeric carbohydrates differing in bioavailability¹⁷—which we had experimentally injected into the flumes. Average uptake of glucose was significantly higher than arabinose in both the slow (2.5-fold, $p < 0.001$, d.f. = 26) and fast (2.3-fold, $p < 0.001$, d.f. = 26) flow treatment, and both monomers showed trends of increasing uptake as biofilms grew (Supplementary Information). However, as biofilms grew, both the absolute and relative uptake rates of arabinose increased, that is

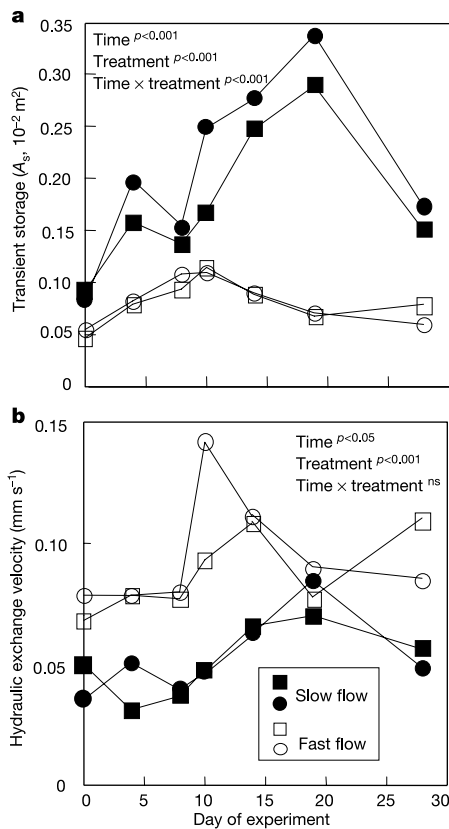


Figure 2 Temporal dynamics of the transient storage zone as A_s (a) and the vertical exchange velocity between the water column and the transient storage (b).

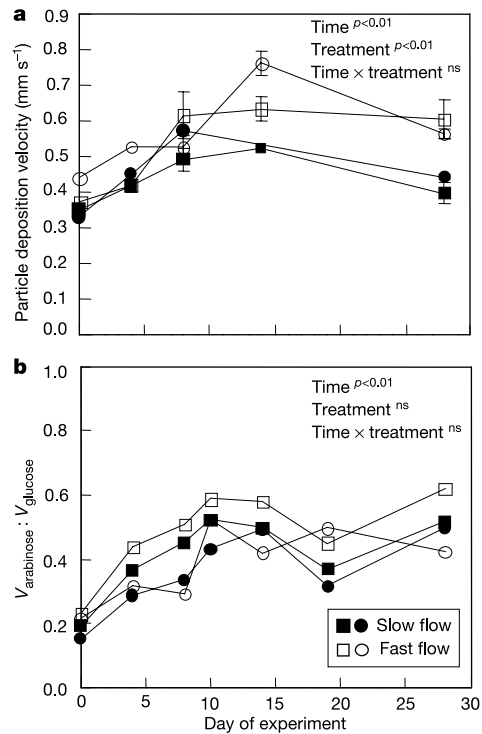


Figure 3 Temporal dynamics of the deposition velocity of suspended organic particles (a) and of the ratio between the mass transfer coefficients for arabinose and glucose (b). Error bars in a indicate the s.d. of the mean of two to five independent particle injections.

$V_{\text{arabinose}}:V_{\text{glucose}}$ increased (Fig. 3b). Thus, biofilm development affected mass transfer, which influenced the relative uptake of substrates differing in bioavailability. These data illustrate the general phenomenon that as transport of solutes from the water column into the biofilm becomes limiting, the susceptibility of a molecule to metabolism shifts from its intrinsic biological lability to the ability to diffuse into the biofilm. Depending on the developmental stage therefore, biofilms reduce the differences in the apparent bioavailability of substrates and compress the longitudinal coupling of substrate production and consumption to shorter distances within a stream reach.

Underlying these mass transfer processes and uptake kinetics is the physical structure of a biofilm¹. Recent work^{11,18} has contradicted the traditional view of biofilms as homogeneous structures subject to diffusion limitation of external and internal mass transport by demonstrating their heterogeneous architecture with channel networks, mushroom-shaped protuberances and oscillating streamers. Such structural heterogeneity presents modelling challenges and suggests that some internal transport may be advective¹⁸. Our experimental measurements of uptake ratios proved useful in assessing the influence of complex structures on transport and uptake kinetics. We found that the $V_{\text{arabinose}}:V_{\text{glucose}}$ ratio not only increased with bacterial abundance (log-phase: $r^2 = 0.90$, d.f. = 16, $p < 0.001$) and biofilm density ($r^2 = 0.67$, d.f. = 7, $p < 0.01$), parameters that should clearly induce transport limitation, but also decreased with biofilm porosity ($r^2 = 0.64$, d.f. = 8, $p < 0.01$) and fragmentation ($r^2 = 0.41$, d.f. = 8, $p < 0.05$), factors that should enhance mass transport. In fact, elevated porosity translates into a larger channel system that favours advective mass transport¹⁸ whereas highly fragmented biofilm clusters with large surface to volume ratios may decrease the average diffusive path length of a substrate molecule from the bulk liquid to cells within a biofilm cluster¹⁹.

Our results highlight the significance of microscale coupling between biofilm structure and function for stream ecosystem biogeochemistry. This focus complements previous considerations of dynamics operating only at the scale of stream reaches^{4,5,8} and is a prerequisite for successful restoration and preservation practices. Because headwater streams are most vulnerable to human alterations, it is imperative to understand the contributions of microbial biofilms to these ecosystems. □

Methods

Cultivation of biofilms

Biofilms were cultivated in four streamside flume mesocosms (length, 30 m; width, 0.30 m; depth, 0.30 m) adjacent to the White Clay Creek (WCC, Stroud Water Research Center). Flumes were scaled to simulate stream natural dynamics and were continuously fed in a once-through mode with raw stream water. Flume slopes were adjusted to 0.0021 and 0.024 m m⁻¹ yielding open channel flow velocity treatments in duplicate with 0.065 ± 0.003 and 0.23 ± 0.005 m s⁻¹, respectively, which translate into the dimensionless Reynolds numbers of 1,869 ± 190 and 7,559 ± 68, respectively. Flumes were packed with the same clean, biofilm-free sediment (median grain size, 20.9 ± 0.8 mm) containing small, unglazed ceramic tiles for the analysis of microbial parameters. Biofilm parameters were monitored every 2 to 3 days on randomly sampled ceramic tiles during the 30-day experiment.

Microscopy and microbial biomass

Confocal scanning laser microscopy and image analysis (Arc-View 2.2, ESRI) of cryosections were used to describe the micro-architecture of biofilms²⁰. Bacteria and certain exopolysaccharides were stained with SYTO 13 and Concanavalin-A Texas Red, respectively²¹. Biofilm porosity was determined as the ratio of the void surface area to the total cross-sectional surface area of cryosections. Sinuosity of the biofilm surface was determined as the ratio between the curvilinear and the linear distance between two given points of the biofilm front²⁰. Biofilm fragmentation was measured as the ratio between the perimeter and surface area of biofilm clusters. Biofilm density was derived from average thickness and total mass estimates. Bacterial abundance, chlorophyll *a* and exopolysaccharides were assayed as described elsewhere²⁰.

Hydrodynamic exchange

Chloride was injected as a conservative tracer into each flume and we monitored conductivity in flume effluents. Hydrodynamic exchange parameters were estimated by least squares using OTIS-P (ref. 22), an advection-dispersion model that includes transient

storage. Estimated parameters were cross-sectional areas of the transient storage zone A_s (m²) and water column A (m²), flow velocity (m s⁻¹), and the storage zone exchange coefficient α (s⁻¹). The equivalent hydraulic exchange velocity (piston velocity) was calculated as $v = \alpha d$, where d is the average water depth. Biofilm cross-sectional area (m²) in the flumes was calculated from the mean biofilm thickness and the average perimeter of the sediment grains in the mesocosms.

Particle and carbohydrate dynamics

Natural suspended particles were collected from WCC and sieved to retain the 53 to 106 µm fraction. Duplicate or triplicate aliquots were injected into each flume, and the effluent was passed through a 50-µm Nitex net to capture particles in transport. Particle mass was corrected for baseline transport and expressed as dry mass (dried at 100 °C) and ash-free dry mass (4 h, 450 °C).

We injected D-(+)-glucose and D-(-)-arabinose along with chloride into each flume to increase monomeric background concentrations from <10 nM to approximately 200 nM. Injections lasted 20 and 15 min in the slow- and fast-flow treatments, respectively (same as for chloride). Triplicate water samples were collected during the conductivity plateau at an upper station and in the flume effluent, filtered (0.2 µm), and frozen pending analysis by HPLC-PAD²³. Arabinose and glucose concentrations were corrected for background concentration.

The transport distances, S (m), of particles and carbohydrates in the water column before uptake were estimated from $S = L \ln(M_{\text{input}}/M_{\text{output}})$, where L is the flume length and M is the input and output mass, respectively²⁴. We divided the width-specific discharge (equivalent to the product of average velocity and depth) by S to yield the deposition velocity for particles and the mass transfer coefficient (mm s⁻¹) for arabinose and glucose. The mass transfer coefficient corrects for the effects of water depth and velocity on uptake and represents the demand by the streambed microbial community for a given molecule relative to its concentration in the water column.

Data analysis

Two-way analysis of variance (ANOVA) was used to test for effects of flow and time on microbial biomass, hydrodynamics, particle and solute dynamics. Kruskal-Wallis one-way ANOVA was used to test for flow effects on biofilm micro-architectural parameters. Stepwise MLR analysis was used to explore the variation of hydrodynamic exchange parameters and particle deposition velocity. Data are given as mean ± s.d.

Received 12 June; accepted 21 October 2003; doi:10.1038/nature02152.

1. Costerton, J. W., Lewandowski, Z., Caldwell, D. E., Korber, D. R. & Lappin-Scott, H. M. Microbial biofilms. *Annu. Rev. Microbiol.* **49**, 711–745 (1995).
2. Palmer, R. J. & White, D. C. Developmental biology of biofilms: implications for treatment and control. *Trends Microbiol.* **5**, 435–440 (1997).
3. Sutherland, I. W. The biofilm matrix—an immobilized but dynamic microbial environment. *Trends Microbiol.* **9**, 222–227 (2001).
4. Jones, J. B. & Mulholland, P. J. *Streams and Ground Waters* (Academic, San Diego, London, 2000).
5. Peterson, B. J. *et al.* Control of nitrogen export from watersheds by headwater streams. *Science* **292**, 86–90 (2001).
6. Alexander, R. B., Smith, R. A. & Schwarz, G. E. Effect of stream channel size on the delivery of nitrogen to the Gulf of Mexico. *Nature* **403**, 758–761 (2000).
7. Gomi, T., Sidle, R. C. & Richardson, J. S. Understanding processes and downstream linkages of headwater systems. *Bioscience* **52**, 905–916 (2002).
8. Packman, A. I., Brooks, N. H. & Morgan, J. J. A physicochemical model for colloid exchange between a stream and a sand bed with bed forms. *Wat. Resour. Res.* **36**, 2351–2361 (2000).
9. Mulholland, P. J., Steinman, A. D., Marzolf, E. R., Hart, D. R. & DeAngelis, D. L. Effect of periphyton biomass on hydraulic characteristics and nutrient cycling in streams. *Oecologia* **8**, 40–47 (1994).
10. Kim, B. K. & Jackman, A. P. Modeling transient storage and nitrate uptake kinetics in a flume containing a natural periphyton community. *Wat. Resour. Res.* **26**, 505–515 (1990).
11. Kugaprasatham, S., Nagaka, H. & Ohgaki, S. Effect of turbulence on nitrifying biofilms at non-limiting substrate conditions. *Water Res.* **26**, 1629–1638 (1992).
12. Minshall, G. W., Thomas, S. A., Newbold, J. D., Monaghan, M. T. & Cushing, C. E. Physical factors influencing fine organic particle transport and deposition in streams. *J. N. Am. Benthol. Soc.* **19**, 1–16 (2000).
13. Thomas, S. A. *et al.* The influence of particle size on seston deposition in streams. *Limnol. Oceanogr.* **46**, 1415–1424 (2001).
14. Drury, W. J., Characklis, W. G. & Stewart, P. S. Interactions of 1 µm latex particles with *Pseudomonas aeruginosa* biofilms. *Water Res.* **27**, 1119–1126 (1993).
15. Grady, C. P. L. Jr, Daigger, G. T. & Lim, H. C. *Biological Wastewater Treatment* 2nd edn (Marcel Dekker, New York, 1999).
16. Gantzer, C. J., Rittmann, B. E. & Herricks, E. E. Mass transport of biodegradable materials to streambed biofilms. *Water Res.* **22**, 709–723 (1988).
17. Kaplan, L. A. & Newbold, J. D. in *Aquatic Ecosystems Interactivity of Dissolved Organic Matter* (eds Findlay, S. E. G., & Sinsabaugh, R. L.) 97–119 (Academic, San Diego, London, 2003).
18. Picioreanu, C., Van Loosdrecht, M. C. M. & Heijnen, J. J. A theoretical study on the effect of surface roughness on mass transport and transformation in biofilms. *Biotechnol. Bioeng.* **68**, 355–369 (2000).
19. Yang, X. M., Beyenal, H., Harkin, G. & Lewandowski, Z. Quantifying biofilm structure using image analysis. *J. Microbiol. Methods* **39**, 109–119 (2000).
20. Battin, T. J., Kaplan, L. A., Newbold, J. D., Cheng, X. & Hansen, C. Effects of current velocity on the nascent architecture of stream microbial biofilms. *Appl. Environ. Microbiol.* **69**, 5443–5452 (2003).
21. Lawrence, J. R., Neu, T. R. & Swerhorne, G. D. H. Application of multiple parameter imaging for the quantification of algae, bacterial, and exopolymer components of microbial biofilms. *J. Microbiol. Methods* **32**, 253–261 (1998).
22. Runkle, R. L. *One-Dimensional Transport with Inflow and Storage (Oris): A Solute Transport Model for Streams and Rivers*. Water-Resources Investigations Report 98–4018 (US Geological Survey, Denver, 1998).

23. Cheng, X. & Kaplan, L. A. Improved analysis of dissolved carbohydrates in stream water with HPLC-PAD. *Anal. Chem.* **73**, 458–461 (2001).
24. Newbold, J. D., Elwood, J. W., O'Neill, R. V. & Van Winkle, W. Measuring nutrient spiraling in streams. *Can. J. Fish. Aquat. Sci.* **38**, 860–863 (1981).

Supplementary Information accompanies the paper on www.nature.com/nature.

Acknowledgements We thank T. Georgian for insights regarding experimental design and the influence of biofilms on particle deposition; S. Roberts, M. Gentile and X. Cheng for technical assistance; K. Czymbek for CLSM support; and A. I. Packman, R. Sommaruga, G. Singer and J. Blaine for critically reading the manuscript. This work was supported by grants from the Austrian FWF (T.J.B.), the US NSF (L.A.K. and J.D.N.) and the Pennswood Fund for Environmental Research (L.A.K. and J.D.N.).

Competing interests statement The authors declare that they have no competing financial interests.

Correspondence and requests for materials should be addressed to T.J.B. (tomba@pflaphy.pph.univie.ac.at).

Balanced inhibition underlies tuning and sharpens spike timing in auditory cortex

Michael Wehr & Anthony M. Zador

Cold Spring Harbor Laboratory, 1 Bungtown Road, Cold Spring Harbor, New York 11724, USA

Neurons in the primary auditory cortex are tuned to the intensity and specific frequencies of sounds, but the synaptic mechanisms underlying this tuning remain uncertain. Inhibition seems to have a functional role in the formation of cortical receptive fields, because stimuli often suppress similar or neighbouring responses^{1–3}, and pharmacological blockade of inhibition broadens tuning curves^{4,5}. Here we use whole-cell recordings *in vivo* to disentangle the roles of excitatory and inhibitory activity in the tone-evoked responses of single neurons in the auditory cortex. The excitatory and inhibitory receptive fields cover almost exactly the same areas, in contrast to the predictions of classical lateral inhibition models. Thus, although inhibition is typically as strong as excitation, it is not necessary to establish tuning, even in the receptive field surround. However, inhibition and excitation occurred in a precise and stereotyped temporal sequence: an initial barrage of excitatory input was rapidly quenched by inhibition, truncating the spiking response within a few (1–4) milliseconds. Balanced inhibition might thus serve to increase the temporal precision⁶ and thereby reduce the randomness of cortical operation, rather than to increase noise as has been proposed previously⁷.

Receptive fields are shaped by the interaction of excitation and inhibition. In the auditory cortex, indirect measurements of this interaction by extracellular methods^{1–5} have suggested that it follows a classic organization—lateral inhibition—in which stimulation in the receptive field centre elicits excitation, and stimulation in the surround elicits inhibition⁸. Here we have used *in vivo* whole-cell patch-clamp methods to test that model directly by measuring synaptic inputs evoked by pure tones in rat auditory cortical neurons⁹ (Fig. 1). For a subset of neurons (31/62), we improved the isolation of synaptic conductances by blocking action potentials with the fast sodium-channel blocker QX-314.

Tone-evoked synaptic conductance changes were large (Fig. 1c), comparable in magnitude to the largest conductance changes elicited by visual stimulation in area V1 neurons^{10–12}. The true

conductances were almost certainly higher than the values presented here, because voltage escape at the subsynaptic membrane due to electrotonic effects (space-clamp errors) causes an underestimation of synaptic conductances (see Supplementary Information). We

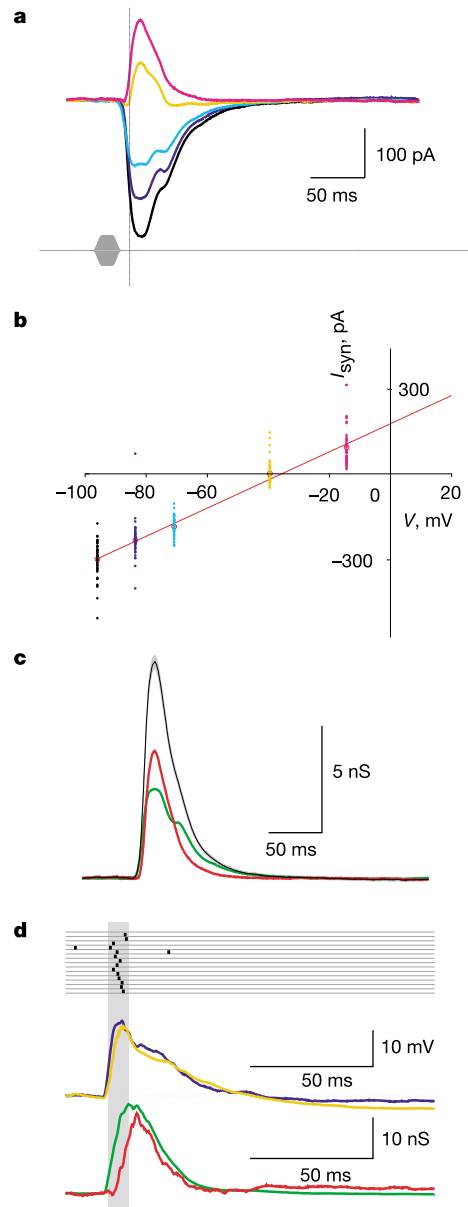


Figure 1 Tones evoked large transient excitatory and inhibitory conductances of comparable magnitudes. **a**, Synaptic currents evoked by a 25-ms tone pip at 1.2 kHz and 66 dB SPL at five holding potentials (48 repetitions). An offset response follows about 25 ms after the onset response. Spikes were blocked with QX-314. **b**, Instantaneous synaptic current-voltage ($-I$) curve. Synaptic currents (coloured dots) are plotted against holding potential (colours as in **a**) for each of the 48 repetitions (means are indicated by red open circles) at the time of half-maximal synaptic conductance (33 ms from tone onset, indicated by the vertical blue line in **a**). The regression slope and x-intercept give, respectively, the instantaneous synaptic conductance (5.0 nS) and synaptic reversal potential (-36 mV). **c**, Continuous synaptic conductance (black line) with 95% regression confidence limits (shaded region), and its decomposition into excitatory (green) and inhibitory (red) conductances. Across all cells for which spikes were blocked, the maximal conductance evoked in each cell was 7.9 ± 9.7 nS, or $46 \pm 54\%$ of resting input conductance ($n = 31$ cells). **d**, In a different cell, for which spikes were not blocked, excitatory and inhibitory conductances (bottom, green and red traces) predicted the spikes (top, raster plot). The predicted (middle, blue trace, see Supplementary Methods) and actual (middle, orange trace) membrane potentials agreed closely.